Calculation of Planck's constant from x-ray crystallography measurements of the crystal structure of Sodium Chloride and polycrystalline Molybdenum

Lab 4 – PHYS2110

Henry Pickersgill - 201004137

X-ray Crystallography

Abstract

Planck's constant, h, is estimated through considering x-ray diffraction with single-crystal Sodium Chloride (NaCl) and the Duane-Hunt relationship. The crystal structures of NaCl and polycrystalline Molybdenum (Mo) are determined through estimating the Miller indices that describe their lattice structures. The result for Planck's constant, $h = (6.1 \pm 0.3) \times 10^{-34} Js$, agrees with the accepted value, $6.63 \times 10^{-34} Js$ [1]. Mo was found to exhibit a body-centred cubic (BCC) structure, agreeing with the known lattice structure; the lattice structure for NaCl was difficult to determine, due to lack of conclusive evidence.

Introduction

Analysing x-ray energy spectra requires an understanding of the ways in which x-rays are produced. Characteristic x-rays are produced by electronic transitions corresponding to specific changes in atomic energy level [2]. Electrons can be displaced when a material is bombarded with high energy particles – this causes an absence in an energy level; therefore, transitions can occur. Due to the quantised nature of atomic energy levels, it is expected that characteristic x-rays possess specific energies, which can be observed as sharp peaks on energy spectra, an x-ray emission spectrum.

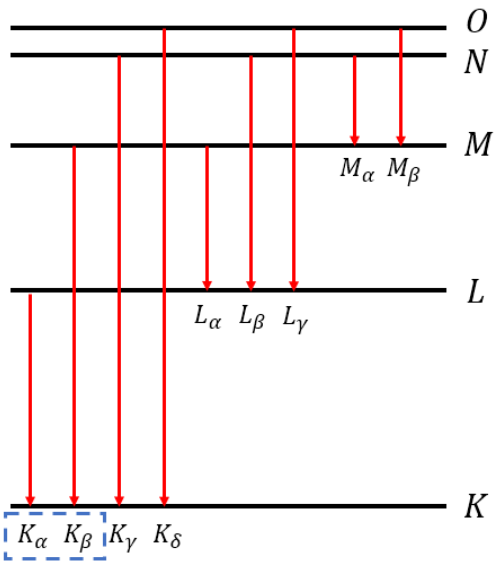

Figure 1: *An illustration of various x-ray producing electron transitions [3].*

Figure 1 demonstrates the possible transitions of an electron within the shells of an atom. The two energy transitions, K_α and K_β, are relatively low energy and very strong spectral lines. These transitions produce peaks that are very easily identifiable in the x-ray energy spectrum. Thus, it is useful to study these emission lines when observing x-ray spectra.

X-rays can also be produced through the deceleration of electrons passing by an atomic nucleus. This results in a continuous spectrum of x-ray energies known as Bremsstrahlung ("braking radiation").

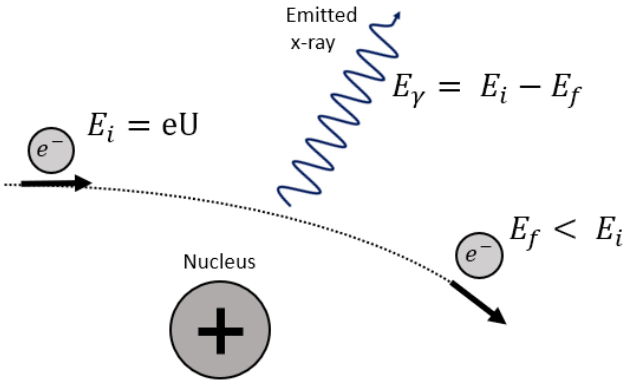

Figure 2: *A graphical depiction of braking radiation; the electron experiences Coulomb attraction and decelerates.*

Figure 2 demonstrates the mechanism of Bremsstrahlung. If we consider the case where the electron is decelerated to a velocity of zero ($E_f = 0$), the *Duane-Hunt law* is obtained. This describes a relationship between the minimum x-ray wavelength, λ_{min}, present in the Bremsstrahlung spectrum, and the x-ray tube accelerating voltage, U. Thus, the Duane-Hunt law is described by equation (1) [3,4]**:**

$$\lambda_{min} = \frac{hc}{eU} \propto \frac{1}{U} \qquad (1),$$

where h = Planck's constant ($6.63 \times 10^{-34} Js$), c = speed of light ($3 \times 10^{8} ms^{-1}$), and e = the elementary unit charge ($1.6 \times 10^{-19} C$).

Planck's constant is a fundamental physical constant encapsulating the quantum nature of photon energies – photons of a *given frequency* have energies in units of h [5]. If the accelerating voltage, U, and minimum x-ray wavelength, λ_{min}, are known, then an initial estimate for h can be generated. A typical x-ray spectrum with the aforementioned features identified is shown in *figure 3* below.

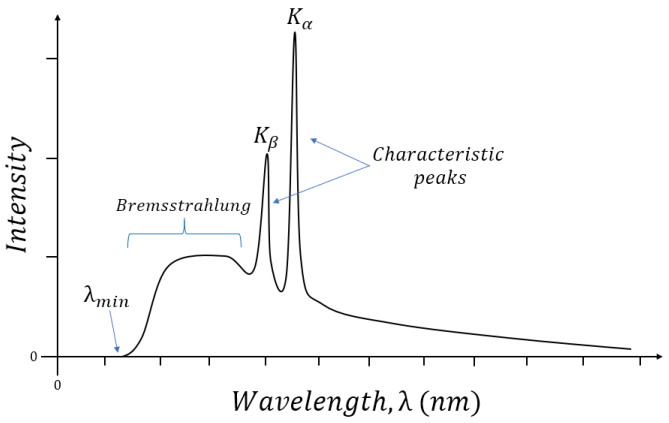

Figure 3: *An x-ray spectrum from a target at* $U = 30kV$

A rigorous approach to estimating h would be to use multiple excitation voltages to obtain a linear relationship between U and λ_{min}, whereby an estimate for h can be generated.

In x-ray diffraction experiments, diffraction is described by *Bragg's Law* [6, p.1252-1253]:

$$\text{path } \Delta = 2x = \boldsymbol{2dsin\theta = n\lambda} \qquad (2)$$

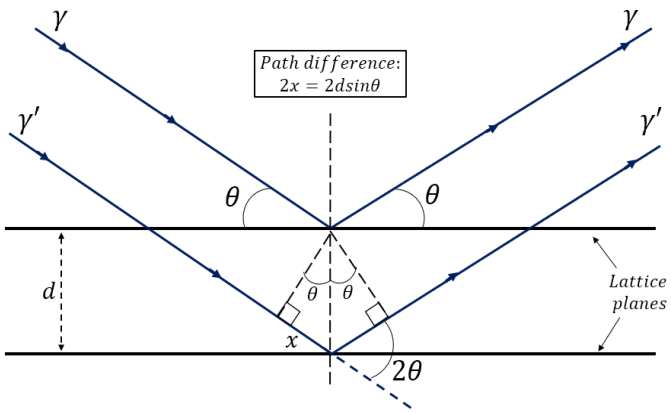

Figure 4*: The interference of two x-ray photons after diffraction from a lattice.*

Figure 4 is a geometrical representation of the path difference between two photons, γ and γ'. Within equation (2), $n = 1,2,3 \ldots$ = order of diffraction, λ = photon wavelength, d = spacing between lattice planes in the material and θ = diffraction angle. (2) describes the condition for *constructive interference*; the superposition of in-phase waves. Bragg's law allows the evaluation of the lattice plane arrangement of a crystal.

Lattice planes are arranged in different ways for a specific crystal, and the arrangement is described using *Miller indices*. Miller indices are a set of three integers, h, k and l, which indicate the set of parallel planes orthogonal to a specific combination of the lattice basis vectors, $\hat{\boldsymbol{a}}_{\boldsymbol{i}}$ [7]. An example is outlined in *figure 5* [8] below.

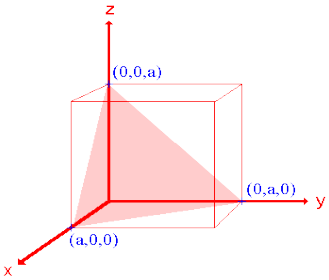

Figure 5a*: A plane corresponding to the indices (111), orthogonal to the vector:*

$$1\hat{\boldsymbol{a}}_x + 1\hat{\boldsymbol{a}}_y + 1\hat{\boldsymbol{a}}_z$$

Symmetry element	Condition for reflection to be present
Primitive lattice	none
Body-centered lattice (BCC)	*h* + *k* + *l* = even
Face-centered lattice (FCC)	*h k l* all odd or even

Figure 5b*: An outline of the selection rules for* h, k *and* l *[9].*

Figure 5a allows a relationship between the lattice constant, a_0 and the lattice spacing, d to be derived (for CUBIC crystals) using simple geometry [3]:

$$d_{hkl} = \frac{a_0}{\sqrt{h^2+k^2+l^2}} \qquad (3)$$

If (2) and (3) are combined, the dependence of Bragg diffraction angle with the Miller indices is generated:

$$\theta_{hkl} = arcsin\left[\frac{\lambda\sqrt{n}}{2a_0}(h^2+k^2+l^2)^{\frac{1}{2}}\right] \qquad (4)$$

Therefore, one can generate a set of predictions for the angular positions of the peaks in an x-ray spectrum. The lattice structure of an unknown material can then be estimated – for example, the structure could be found to be FCC (face-centred

cubic), BCC (body-centred cubic) or neither ($\lambda = 0.7108\text{Å}$ for the Mo target).

Ultimately, the goal of this part of the experiment was to determine the crystal structure of NaCl and Mo. The x-ray apparatus is used to scan a range of angles, θ, to locate Bragg diffraction peaks (where a high probability of x-ray detection is observed). The locations can then be correlated with the predicted location of the peaks, generated from all combinations of h, k and l, to determine the most likely lattice structure. The combination of h, k and l determines whether FCC, BCC or primitive reflections are present, according to *figure 5b* **[9]**.

Experimental Design

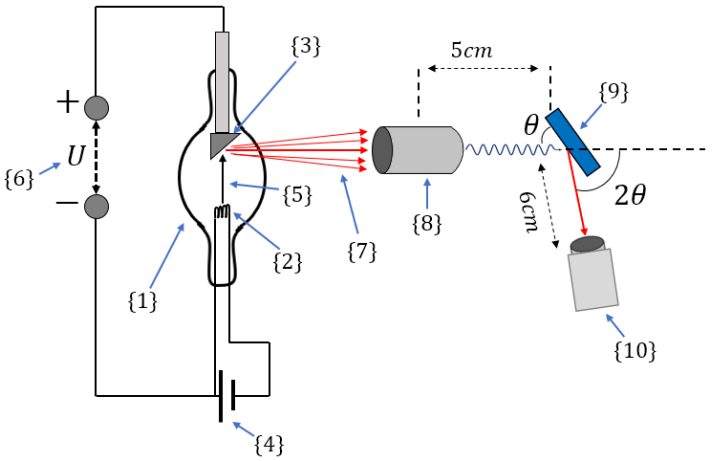

Figure 6: *A schematic diagram of the arrangement of the experimental apparatus.*

The experimental setup is displayed in *figure 6* above. A Roentgen (x-ray) tube {1} consists of a filament, the cathode {2}, and a Mo target, the anode {3}. The cathode is connected in series with a DC power source {4} which heats the filament, releasing electrons {5}. These electrons are accelerated across the high voltage {6} and bombard the Mo target, producing high energy x-rays {7} in the manner described earlier. The Mo target emits x-rays similarly to a point source; therefore, the x-rays pass through a collimator {8}, which acts as a filter, producing a narrow, parallel beam of x-rays. The focused x-rays then collide with the target placed within the target holder {9} and diffract in a way described by Bragg's law (equation (2) and *figure 4*). Importantly, x-rays diffract at an angle 2θ with respect to the detector {10} position, consequently, this is the angle which the apparatus records.

Method – Planck's Constant

For the purposes of this experiment, an NaCl single crystal was secured upon the target holder. The aim was to confirm the relationship between the minimum wavelength, λ_{min}, and the high voltage applied, U as predicted by the Duane-Hunt law (1) and estimate Planck's constant. The apparatus allows the detector to scan freely over a specified range of angles, to search for the characteristic features of the x-ray spectrum. Calibration of the apparatus was performed and required scan parameters [3] were applied. Eight excitation voltages were used in the range: $U = 22$ to $35kV$, and the scan was performed over a short range of angles.

Through analysis of the energy spectra for each of the high voltages, estimates for λ_{min} were generated. In theory, a single value for λ_{min} for a specific high voltage would be present, however, in practice, the spectra showed asymptotic behaviour towards a count rate of zero. Thus, it was particularly difficult to determine precisely when the spectra reached a count rate of zero, therefore, the linear method of determining the wavelength axis intercept (λ_{min}) was utilised.

A relationship between λ_{min} and $^1/_U$ allowed an estimate for h to be calculated using equation (1). The uncertainty in this estimate was determined from the uncertainty in the quantities λ_{min} and U. Uncertainty in U arose from the precision of the x-ray apparatus, and the uncertainty in λ_{min} was calculated from the linear intercept method as described earlier. For the purposes of this experiment, the constant $^e/_c$ was assumed to have negligible experimental uncertainty.

Method – Crystal Structures

This part of the experiment concerned the crystal structures of NaCl and Mo. The aim was to determine whether these materials exhibit FCC, BCC or primitive lattice structures. A Zirconium (Zr) filter was utilised, placed on the left side of the collimator (with reference to *figure 6*). The Zr filter functioned to eliminate the K_β peak for each order, n, from the x-ray spectrum.

Firstly, a sample of polycrystalline Mo [3] was placed upon the target holder. The x-ray apparatus was calibrated and scan parameters, $5° \leq \theta \leq 30°$, were applied. This range was used to ensure observation

of many peaks corresponding to the various Miller indices for planes present within the polycrystal. Firstly, it was required to produce a set of predictions for the angular positions of the K_α peaks, θ_{hkl}. This was achieved through consideration of each possible combination of the Miller indices, $h, k,$ and l, and applying equation (4). A scan was performed to generate the required x-ray spectrum, and the angular positions of eight K_α peaks were recorded. These positions were then compared with the predicted locations.

A sample of powdered NaCl was then placed upon the target holder. This was to ensure the spacing between each single-crystal was minimised [3], as these spaces would scatter x-rays in an unpredictable manner, distorting the spectrum. The predicted angular positions, θ_{hkl}, were calculated for NaCl using equation (4), and a scan was performed within the range $5° \leq \theta \leq 20°$. This was chosen to reduce scanning time, and as it is a large enough range to observe multiple K_α peaks for NaCl x-ray spectra. The angular positions of six K_α peaks were recorded and compared with the predicted locations. For both Mo and NaCl, the angular positions of each peak were difficult to locate precisely. Therefore, Gaussian curves were used to approximate the peak and locate the point of maximum intensity – these points were used as the θ values. Attempts to deduce the lattice structures of Mo and NaCl using the rules outlined in *figure 5b* were made.

Results

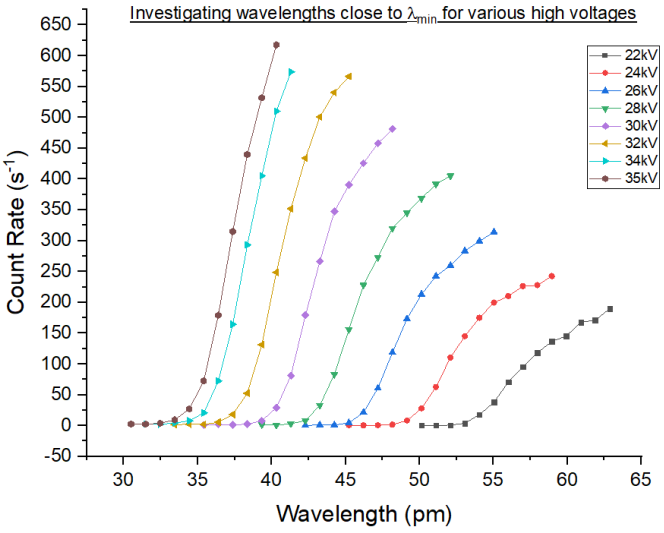

Figure 7*: Portions of the x-ray spectra for various high voltages.*

The relationship between λ_{min} and U was determined and is displayed in *figure 7.* Using the Duane-Hunt law, an estimate for Planck's constant was calculated:

$$h = (6.1 \pm 0.3) \times 10^{-34}\text{Js}$$

The predicted peak angular positions were very accurate for polycrystalline Mo. *Figure 8* below shows the eight observed peaks along with the corresponding Miller indices responsible for each peak.

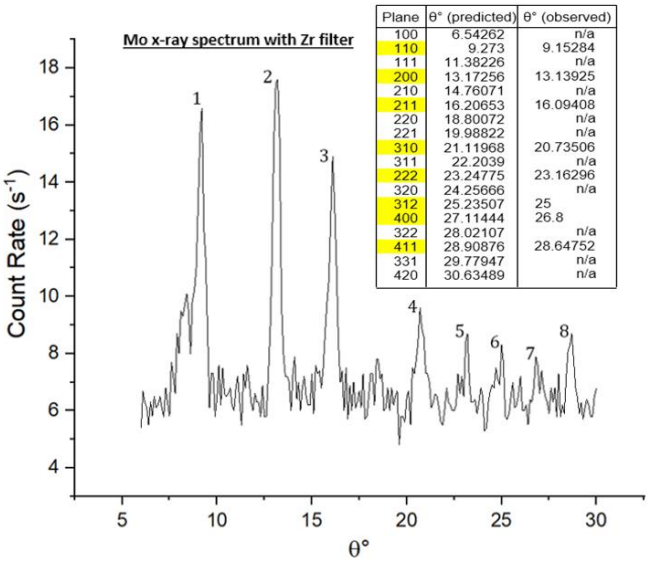

Figure 8: *Eight recorded K_α peaks for the Mo sample. Predicted and observed angular positions are shown.*

Figure 8 provides ample evidence to conclude, using the conditions in *figure 5b*, that Mo exhibits body-centred cubic (BCC) lattice structures. The peak positions predicted within the range specified for NaCl were all located in the x-ray spectrum.

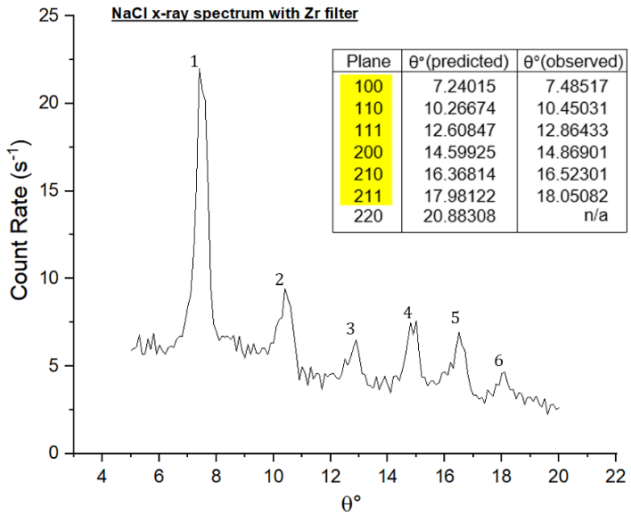

Figure 9*: Six recorded K_α peaks for the powdered NaCl sample. Predicted and observed angular positions are shown.*

Figure 9 shows the six observed peaks and the planes corresponding to each peak. *Figure 9* does not provide enough evidence, however, to conclude the nature of the lattice structure of NaCl. Each peak predicted, within the range $0 \leq \theta \leq 20°$, was observed, and the conditions in *figure 5b* suggest NaCl exhibits all of BCC, FCC and primitive lattice structures.

Discussion

Figure 7 confirms the Duane-Hunt relationship between the minimum x-ray wavelength and the excitation voltage. However, as discussed previously, where exactly a count rate of zero occurs was difficult to determine. A linear plot was generated for each curve to estimate the horizontal axis intercept; although, this method may be considered inaccurate in this circumstance. This is because many different linear plots seemed to fit the data well for each curve, and only four points were used for each plot. The final estimate for Planck's constant showed a slight discrepancy from the accepted value, likely due to some systematic error within the experimental setup. Additionally, no repeats were taken for each excitation voltage, thus, the estimate for h was generated from single sets of data for each value of U. The uncertainty in h was also largely affected by the uncertainty in the exact position of λ_{min}.

Observation of the Bragg diffraction peaks in the x-ray spectra of polycrystalline Mo and single-crystal NaCl provided vastly different conclusions. The angular positions of the peaks for Mo were very accurate with respect to the predicted positions and allowed a confident conclusion to be made – polycrystalline Mo exhibits BCC lattice structures. The angular positions of the observed peaks for NaCl were also very accurate with respect to predicted positions. However, all six predicted Bragg peaks within the range used in the scan were observed. Therefore, it was difficult to deduce which lattice structure is mostly present within NaCl using the conditions in *figure 5b*.

Conclusion

The study of this experiment was the use of x-ray spectroscopy in determining the properties of crystalline materials. Additionally, the experiment generated an estimate for Planck's constant, h; the constant which describes the quantisation of energy. Using x-ray spectroscopy apparatus, the required energy spectra (*figure 3*) was generated for two materials – polycrystalline Molybdenum (Mo) and single-crystal Sodium Chloride (NaCl). These spectra display features key to understanding the energy levels within the atoms of each material. The minimum possible x-ray emission wavelength λ_{min} was studied through consideration of the continuous part of the spectrum (Bremsstrahlung). Application of various excitation voltages, U, allowed the Duane-Hunt law to be confirmed. From this law, the value for Planck's constant was determined as $h = (6.1 \pm 0.3) \times 10^{-34} Js$. The accepted value for this quantity is $6.63 \times 10^{-34} Js$. This corresponds to an 8% difference. Therefore, it can be concluded that the estimate agrees with the known value for h. The sharp peak features of each spectrum, which correspond to characteristic x-ray energies, were studied. The aim was to record the angular positions of these peaks and compare the observations with predicted peak locations. These peak locations were generated from each possible combination of Miller indices. It was concluded that polycrystalline Mo exhibits a body-centred cubic structure (BCC). It was difficult to deduce the lattice structure of NaCl accurately – it was found to contain body-centred, face-centred and primitive cubic structures. The lattice structure of NaCl is thought to be predominantly FCC (see [10], [6, p.1282] and [11]). This suggests that there were clearly some problems with the experimental method or some variables that could be adjusted to help confirm the results.

One problem with utilising the Duane-Hunt law is the fundamentally quantum nature of electrons. An electron can never completely lose its energy, which equation (1) relies on, and therefore the asymptotic behaviour is observed in the x-ray spectrum. Thus, this contributed to the difficulty in determining the exact position of λ_{min}. This explains the relative uncertainty in the calculation of h, as the uncertainties in U, e and c are negligible in comparison.

One can confidently assume the x-ray apparatus was correctly configured. Known peak locations for NaCl were used to calibrate the position of the target holder and detector to a miniscule uncertainty. Hence, it is assumed that the lack of evidence for the lattice structure of NaCl is due to experimental design, as opposed to equipment setup. The scan range for NaCl was chosen as $5° \leq \theta \leq 20°$, and this was clearly not sufficient for the aim of the experiment. The peak locations matched theoretical predictions, however, this did not allow any

conclusions to be made about the structure of NaCl. A larger range of angles should be utilised, to ensure some predicted peaks are **not** observed. This would help in drawing conclusions more effectively. Fundamentally, the validity of the results could be improved through repeats. One run was performed for each excitation voltage, due to time constraints; perhaps a more precise value for Planck's constant would be generated through repeating and averaging.

References

[1] Augustyn A, The Editors of Encyclopaedia Britannica. (2019). *Planck's Constant*. [Online]. [Accessed 02/05/2019]. Available from: https://www.britannica.com/science/Plancks-constant

[2] Merzbacher, E., Lewis, H. (1958). X-ray Production by Heavy Charged Particles. *Corpuscles and Radiation in Matter II / Korpuskeln und Strahlung in Materie II*, pp.166-192.

[3] Leeds University School of Physics and Astronomy. (2018-2019). *PHYS 2060 and PHYS2110 Guidance and Scripts Handbook*. pp.31-42

[4] LEYBOLD DIDACTIC GMBH. (2019). *Leybold Physics Leaflets, P6.3.3.3*. Atomic and Nuclear Physics - Duane-Hunt relation and determination of Planck's constant.

[5] Perkovac, M. (2017). Planck's h and Structural Constant s_0. *Journal of Modern Physics*, **8**(3), pp.425-438.

[6] Tipler P. A., Mosca G. (2007). *Physics for Scientists and Engineers (with Modern Physics) 6th Edition.* W H. Freeman.

[7] Frank, F. (1965). On Miller–Bravais indices and four-dimensional vectors. *Acta Crystallographica*, **18**(5), pp.862-866.

[8] Nix, R. (2018). *Miller Indices (hkl)*. [Online]. [Accessed 27/04/2019]. Available from: https://chem.libretexts.org/Bookshelves/Physical_and_Theoretical_Chemistry_Textbook_Maps/Supplemental_Modules_(Physical_and_Theoretical_Chemistry)/Surface_Science/1%3A_Structure_of_Solid_Surfaces/1.1%3A_Introduction/Miller_Indices_(hkl)

[9] Lufaso, M. (2019). *Chapter 2 – Physical Methods for Characterizing Solids.* [Online]. [Accessed 28/04/2019]. Available from: https://chem.libretexts.org/Bookshelves/Physical_and_Theoretical_Chemistry_Textbook_Maps/Supplemental_Modules_(Physical_and_Theoretical_Chemistry)/Surface_Science/1%3A_Structure_of_Solid_Surfaces/1.1%3A_Introduction/Miller_Indices_(hkl)

[10] Brillouin, L. (1946). *Wave Propagation in Periodic Structures*. Mineola, New York, Dover Publications inc, p.16.

[11] Khadeeva, L., Dmitriev, S. (2010). Discrete breathers in crystals with NaCl structure. *Physical Review B*, **81**(21), p.1.